Available online at www.sciencedirect.com
SCIENCE DIRECT
Polymer 46 (2005) 661–669
polymer
www.elsevier.com/locate/polymer

Study of the porous network developed during curing of thermoset blends containing low molar weight saturated polyester

N. Boyard[a], M. Vayer[a,*], C. Sinturel[a], R. Erre[a], P. Levitz[b]

[a]Centre de Recherche sur la Matière Divisée, 1 B rue de la Férollerie, 45071 Orleans Cedex 02, France
[b]Laboratoire de Physique de la Matière Condensée, UMR 7643, Ecole Polytechnique, Route de Saclay, 91128 Palaiseau, France

Received 17 May 2004; received in revised form 9 November 2004; accepted 22 November 2004
Available online 13 December 2004

Abstract

Polymerisation of unsaturated polyester/styrene blend added with a thermoplastic additive leads to the formation of a porous biphasic polymer network. In this paper, the porous medium was specifically studied by TEM associated with images analysis by chord length distribution and small angle X-ray scattering (SAXS). When the molar weight and/or the amount of low profile additive (LPA) are sufficient to ensure porosity higher than 2%, chord length distribution can be performed and is characteristic of a Debye random medium and Porod's law was observed in SAXS. The lengths deduced from Porod's law are similar to those observed for Debye random regime and are lower than 50 nm. These characteristics are closely related to the processes happening during curing and especially to the phase separation. For less porous samples, deviation from Porod's law was observed and could be attributed to additional scattering intensity coming from concentration fluctuations within polymer matrix. For nonporous samples, scattering intensity was only due to concentration fluctuations.

Keywords: Porosity; Chord distribution; Unsaturated polyester

1. Introduction

Crosslinking of thermoset blends based on unsaturated polyester (UP) and styrene (ST) induces a high degree of polymerization shrinkage (normally 7–10%) [1–4] compared to epoxy resins. In order to compensate this shrinkage, low profile additive (LPA) thermoplastic polymer is added. During curing, different phenomena take place: crosslinking reaction, phase separation between a UP rich-phase and LPA rich-phase, gelation, shrinkage (related to the reduction of steric hindrance of the macromolecular system with conversion degree) and stresses relaxation. The stresses relaxation proceeds generally by pores formation. The final developed architecture results from the combination of all these phenomena [2,5]. The most influent parameters on the morphology are the amount and the nature of the thermoplastic additive [5–7] and the procedure parameters (temperature, pressure) [8,9].

For initially miscible blends UP/St/LPA, the final morphology is a biphasic porous network formed by a spinodal decomposition, which can be frozen in the first stage (co-continuous structure) [2,10,11] or in the later stages (growth of the structure or coarsening process) [2,12]. This morphology is generally described as a two-phase morphology (microparticles of cured UP connected in a macro-network and surrounded by LPA). Although the final morphology is well described in term of bulk morphology and some of the related phenomena (phase separation) have been investigated, the description of the porous medium [13–15] is poorly documented. However, accurate analysis of the porous medium generated by stresses relaxation process is very important since numerous properties (mechanical, transport, surface aspect …) depend strongly on the geometry of the porous medium.

In this paper we investigate the porous network of thermoset samples containing low molar weight saturated polyester as LPA. Considering our experimental conditions (heating ramp up to 110 °C) and blend compositions, the bulk morphology is described as particles sized between 50

* Corresponding author. Tel.: +33 2 38 494737; fax: +33 2 38 417043.
E-mail address: marylene.vayer@univ-orleans.fr (M. Vayer).

0032-3861/$ - see front matter © 2004 Elsevier Ltd. All rights reserved.
doi:10.1016/j.polymer.2004.11.094

and 70 nm surrounded by LPA and linked together in aggregates sizing between 500 and 600 nm into a 3D network [11]. The phase separation has been shown to be a spinodal decomposition frozen in the early stage [11] for a conversion degree which cannot be higher than 0.1 [3]. At this step the bulk network is biphasic, co-continuous and with a correlation length about 120 nm. A macroscopic approach of porosity formation has been provided by dilatometric studies, which show that pores are formed much after the phase separation for a conversion degree higher than 0.5 [4]. This paper will consequently focus on the description by TEM and SAXS of the final porous medium. The porous medium obtained using a more classical additive such as poly(vinyl acetate) (PVAc) will be also investigated and compared to those obtained with LPA. The characteristics of the porosity (morphology and characteristic of the porous interface) will be correlated to the phase separation characteristics.

2. Materials and methods

2.1. Materials

The thermoset blends were composed of: (i) an unsaturated polyester prepolymer (UP); (ii) a curing agent (Styrene referred in the text as ST) (iii) a low profile additive (LPA); (iv) a polymerization initiator (tertiobutyl perhexanoate ethyl-2). The UP prepolymer was Palapreg P18-03 from DSM Composite Resins, made from maleic anhydride, propylene glycol and neo-pentyl glycol. Provided resin P18-03 contained 67.5 wt% UP and 32.5 wt% styrene. The C=C molar ratio (styrene)/(unsaturated polyester prepolymer) in the prepared formulations was adjusted to a value of 2.0 by adding styrene. Non-commercial saturated polyesters (noted LPA1 and LPA2), made and provided by Cray Valley, were employed as thermoplastic additives. They were based on adipic acid, propylene glycol and ethylene glycol. These saturated polyesters were named LPA1 ($M_n = 1140$ g mol^{-1}, $M_w = 2020$ g mol^{-1}) and LPA2 ($M_n = 2690$ g mol^{-1}, $M_w = 6420$ g mol^{-1}).For comparison purpose, poly(vinyl acetate) (Neulon 8000, $M_n = 100\,000$ g mol^{-1}) from Dow Chemicals was used and referred as PVAc. Neulon 8000 contained 57.2 5 wt% of styrene. The molar weights of these polymers were determined by GPC using poly-styrene calibration standard. All the materials were employed as received, without further purification. Tertiobutyl perhexanoate ethyl-2 (TBPEH—1 wt% of UP/St) from Peroxide-Chemie GmbH was used as polymerisation initiator.

The LPA contents were 5, 15, 25% of the total weight of the blend (UP/ST/LPA). A blend without LPA was prepared. For PVAc only one sample containing 15% PVAc was prepared. Samples were named by their LPA percentage following by the type of LPA except for the blend without LPA named UPST. As example, a sample containing 15% of LPA2 was named 15% LPA2.

For TEM analysis, cylindrical samples (diameter: 50 mm, thickness: 4 mm) were moulded by compression using a Derek press in a stainless steel mould. The polished female part was heated at 150 °C and the punching die at 135 °C. Pressure applied on composite was 10 MPa and the curing time was 100 s.

For SAXS analysis, squared samples (length, 20 mm; thickness, 0.9 mm) were moulded in a home-made PTFE mould in an oven at 110 °C during 15 min.

2.2. Instrumentation and procedures

2.2.1. Measurement of the macroscopic porosity

The macroscopic porosity was determined by immersion: cured samples were weighted in air m_{air} and distilled water m_{water}. The experimental density d_{exp} was then determined using the relation

$$d_{exp} = \frac{m_{air}}{m_{air} - m_{water}} d_{water} \quad (1)$$

The macroscopic porosity P was obtained from the values of experimental d_{exp} and theoretical d_{th} densities using the relation

$$P = \frac{d_{th} - d_{exp}}{d_{th}} \quad (2)$$

with

$$1/d_{th} = 1/\sum_{i=1}^{n} \frac{W_i}{d_i}.$$

d_{th} was calculated from the weight fraction (W_i) and the density (d_i) of i phase, and n is the total number of phases in the sample The experimental density of neat cured resin (UP + ST) was found to be 1.157 whereas the densities of the bulk thermoplastic additives LPA1 and LPA2 were provided by the supplier and estimated to 1.250 in both cases. The density of pure PVAc additive was 1.155 and was calculated from the density of the commercial product (d = 0.994), where PVAc is diluted in styrene (styrene density = 0.900). Using this technique, the open porosity cannot be taken into account since water can flow into this later. Comparison between the densities determined by relation (1) and those determined by weighing samples of known dimensions, allows us to conclude that the open porosity was negligible.

2.2.2. Transmission electron microscopy (TEM)

TEM was performed on a Philipps CM20 where an acceleration voltage of 120 kV and a resolution of 0.7 nm were used. The electron gun was equipped with a LaB_6 monocristal for a high brightness. The samples for transmission electron microscopy were microtomed to a thickness of about 50 nm at room temperature and placed on a TEM grid. The samples cut were stained using RuO_4 to optimise the contrast between the phases and to limit

deformations of the microtomed samples in the electron beam. The RuO_4 staining solution was prepared using NaOCl solution and $RuCl_3$ following a procedure described in the literature by Brown and Butler [16]. After microtomy, the samples on the TEM grids and a open vial containing the RuO_4 solution (3 ml) were placed together in a closed Petri box. The samples were thus exposed to RuO_4 vapour during 3 min, which was found to be the optimal staining duration.

Images were captured for various magnifications ($\times$ 6000 to $\times$30 000) and digitalized (1 pixel corresponds to 11 nm for the magnification $\times$6000) for analysis with chords length distribution.

2.2.3. Ultra small angle X-ray scattering (USAXS)

Small-angle scattering data were collected on a set up designed by Lambard et al. (DRECAM/SCM/ Groupe Chimie de la Matière Ultradivisée, CEA Saclay, France) [17]. This includes an 18 kW rotating anode X-ray generator with copper target in order to work with K_α radiation ($\lambda=$ 0.154 nm). Two pairs of horizontal and vertical slits focus the beam on a first crystal (the monochromator) giving a large collimated beam with very small horizontal divergence. The beam (1 or 2 mm) is centred on the second axis holding the sample. The beam outgoing the sample was analysed by a second multiple reflection crystal (the analyzer). The scattered light and the direct beam were measured with a scintillator associated with a photomultiplier. This measurement was done by rotating the whole detection system using a movement 2θ around the sample axis. The scattering q vector was spanned from 7.0×10^{-4} Å^{-1} to 9×10^{-2} Å^{-1}. After subtracting the background scattering curve (for sample holder), the scattering curve was corrected from transmission and desmeared to get the diffusion pattern related to the punctual geometry of the incident beam [17].

2.3. Theoretical background

2.3.1. Chord analysis

The concept of 'chord-length distribution' introduced by Mering and Tchoubar [18] is used to characterize two-phase system in particular porous materials on stereological principles. A chord is defined as a segment that belongs either to the pore or to the solid and has both ends on the interface. In this approach, the density of each point can take only two values 0 and ρ (electronic density of the cured blend) implying a sharp boundary interface. The chord size distribution 'in number' is related to the probability of having a chord size between r and $r+\mathrm{d}r$, lying entirely in one phase. Chord distribution functions are involved in the expression of the second derivative of the bulk autocorrelation function and then strongly related to small angle scattering [19].

The porous network was investigated through 2D random sections of the 3D sample assuming that the sample is isotropic. We used the chord distribution of the pore network $f_p(r)$ and of the solid matter $f_m(r)$. These distributions give an objective description of an average pore. 3D parameters such as porosity (Φ) and specific area per volume S/V can be estimated from the mean chord lengths $\bar{l}_m$ and $\bar{l}_p$ via

$$\Phi = \frac{\bar{l}_p}{\bar{l}_m + \bar{l}_p} \tag{3}$$

and

$$\frac{S}{V} = \frac{4\Phi}{\bar{l}_p} = \frac{4(1-\Phi)}{\bar{l}_m} \tag{4}$$

with

$$\bar{l}_m = \int_0^\infty r f_m(r)\mathrm{d}r \quad \bar{l}_p = \int_0^\infty r f_p(r)\mathrm{d}r.$$

A characteristic length $\bar{d}$ is defined by

$$\frac{1}{\bar{d}} = \frac{1}{\bar{l}_m} + \frac{1}{\bar{l}_p}. \tag{5}$$

For chord-length distribution analysis, we neglected the superposition of different morphological features induced by the thickness of the sample.

2.3.2. Chord distribution in a Debye random system

A two-phase Debye random system is described as 'a distribution of holes of random shape and size' [20]. In this case, the chord-length distribution functions in number for pore and mass exhibit an exponential variation [21] and can be written as

$$f_m(r) = \frac{1}{\bar{l}_m}\exp\left(\frac{-r}{\bar{l}_m}\right) \text{ and } f_p(r) = \frac{1}{\bar{l}_p}\exp\left(\frac{-r}{\bar{l}_p}\right) \tag{6}$$

where $\bar{l}_m$ and $\bar{l}_p$ are the mean chord-lengths for mass and pore.

The autocorrelation function of this system [19,22] is

$$\gamma(r) = \exp(-r/a) \tag{7}$$

and consequently leads the well known Debye expression of scattered intensity [19,22]:

$$I(q) \propto \frac{1}{(1+aq^2)^2} \tag{8}$$

a is a measure of the extension of the inhomogeneity and is called by Debye [22] correlation length. It corresponds to $\bar{d}$ given in the Eq. (5).

When a Debye randomness is considered in the low r-range, Eq. (6) exhibits a negative slope and a non-zero value for $r=0$. Such results involve a strong interfacial angularity [18]. For a real system with a flat interface, the chord distributions scale as r for small r-values. The positive slope of this linear relationship is directly related to the curvature properties of the interface.

2.3.3. USAXS data analysis

For high q-values ($q^{-1} \ll R$) and for flat interface between two phases of constant electronic density, Porod showed that the scattered intensity $I(q)$ is proportional to q^{-4}:

$$\lim_{q\to\infty} I(q) = 2\pi(\Delta\rho)^2 \frac{S}{V} q^{-4} \tag{9}$$

where $(\Delta\rho)$ is the electronic density difference between the phases and S/V is the specific area per volume which was previously defined.

The invariant Q of the scattered beam for a two-phase system is defined as follows:

$$Q = \int_0^\infty q^2 I(q)\mathrm{d}q = 2\pi^2(\Delta\rho)^2\phi(1-\phi) \tag{10}$$

Obtaining data over all scattering vectors is experimentally highly difficult and thus only a partial invariant, Q^* will be determined directly from experimental data:

$$Q^* = \int_{q_{\min}}^{q_{\max}} q^2 I(q)\mathrm{d}q \approx 2\pi^2(\Delta\rho)^2\phi(1-\phi) \tag{11}$$

The values of $q_{\min}$ and $q_{\max}$ were 7×10^{-4} and 0.09 Å^{-1}, respectively. We verified by extrapolating the plot $q^2 I$ versus q that the difference between Q and Q^* did not exceed 2%. The error on the invariant Q is then quite low.

If the Porod's law can be applied combining Eqs. (9) and (11) leads to

$$\frac{4(1-\phi)\phi}{S/V} = \frac{4Q^*}{\pi \times \lim(q^4 I)_{q\to q_{\max}}} \tag{12}$$

Porod introduced $l_C = 4\phi(1-\phi)V/S$ as a characteristic length of the system called Porod length which has to be compared with the length defined in Eq. (5).

In some cases strong deviations from the usual Porod law in the 'high' q regime can be observed [23–26]. Deviation from Porod law can either positive (>-4) or negative (<-4).

Negative deviation has been reported in the cases of fuzzy interfacial zones where density transition from one phase to the other is progressive. This case of diffuse interfaces was analyzed by Ruland in 1970 assuming that the density transition zone follows a Gaussian profile [24]. In such a case, $q^4 I(q)$ evolves as $1-aq^2$ and exhibits a negative slope.

In the case of positive deviation two explanations are generally given. The first one corresponds to rough interface and has been analyzed in the work of Sinha et al. [25]. In this situation, $q^4 I(q)$ evolves as $1+aq^{(\mathrm{d}s-2)}$ with $3>\mathrm{d}s>2$. A continuous curve with a positive slope is then observed, associated to a characteristics exponent ranging between 3 and 4. In the second case, a density fluctuation within the bulk phases, discussed by Ruland [24] and more recently by Smarsly et al. [25] can interfere with the Porod law providing a positive deviation in the $q^4 I(q)$ versus q^2 plots.

3. Results

3.1. Characterization of the porosity by TEM associated with chord-length distribution analysis

Porosity was observed by TEM for all the samples. An example for 25% LPA2 is shown in Fig. 1(a). Porosity (in white) resulting from local stresses relaxation and responsible for shrinkage compensation can be clearly distinguished from polymer phases (in gray). The pores exhibit complex shapes, which demonstrate the random stresses release during crosslinking. Their distributions in the bulk appear homogeneous. In order to quantify the porosity (size distribution and characteristic length) we chose to use chord-length distributions analysis [19].

The pore and mass chord-length distributions were calculated from the digitized images (Fig. 1(b)) for all the samples except 5% LPA1 and 15% LPA1 although the samples revealed porosity. In these latter two cases, the pores are too small (less than 2 pixels) and not enough numerous to allow a meaningful chord-length distribution analysis. An example of pore and mass chord-length distribution for 25% LPA2 is shown in Fig. 2. Similar distributions shapes were found for the LPA1 and LPA2

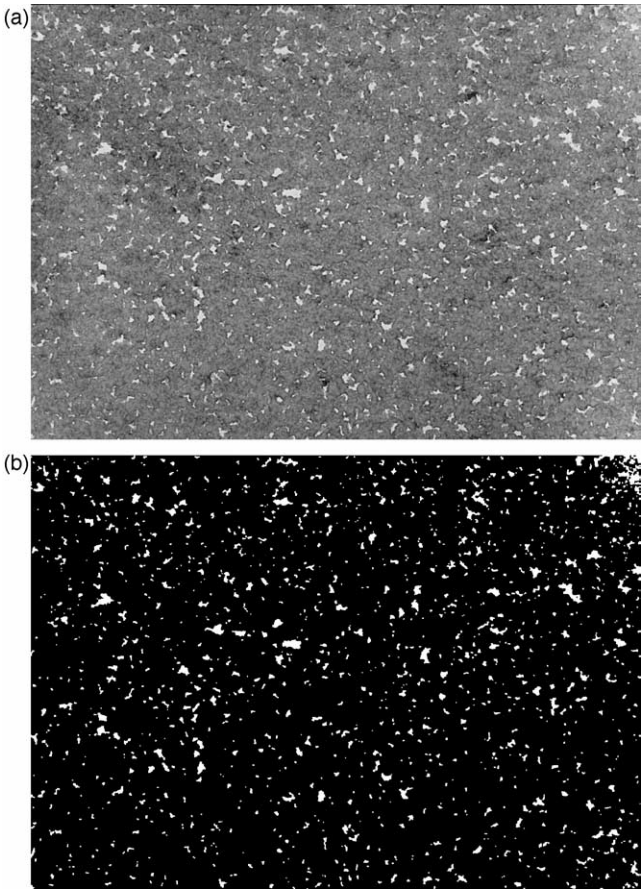

Fig. 1. (a) TEM micrograph of a 25% LPA2 sample. (b) Corresponding digitized image. Size of the image: 8.9 μm×14.5 μm.

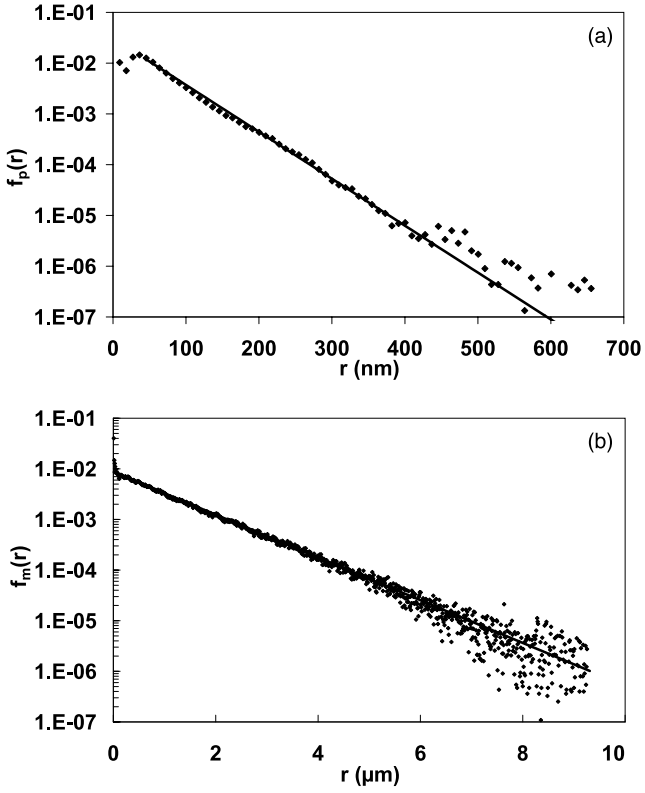

Fig. 2. Pore (a) and mass (b) chord-length distribution functions (log-linear scale) from digitized image of 25% LPA2 sample.

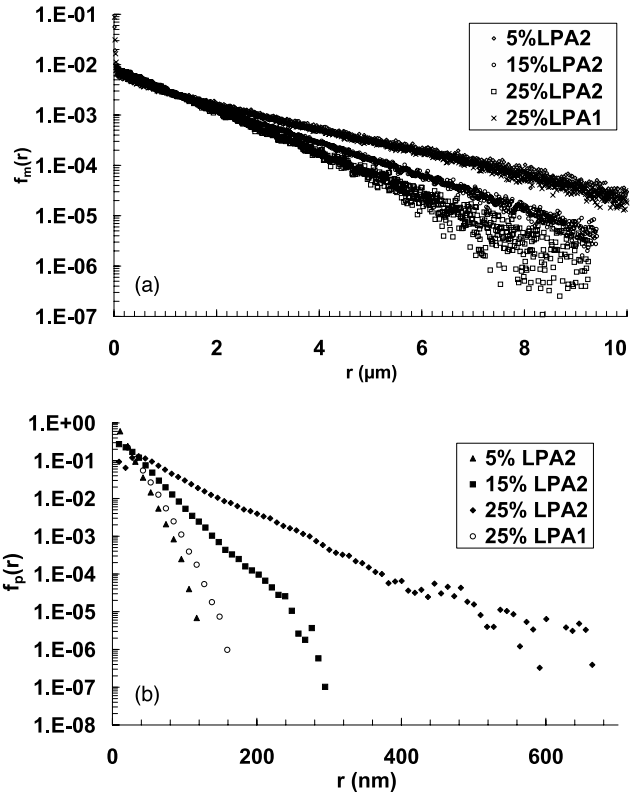

Fig. 3. Comparison of the mass (a) and pore (b) chord distribution functions (log-linear scale) for 5, 15, 25% LPA2 and 25% LPA1.

samples (Fig. 3). Table 1 indicates the range of pore chord-length observed for the various samples. The chords lower than 2 pixels (r less than 20 nm) are not considered, since they have no physical meaning due to the limit of image resolution. The maximal value depends on the LPA type and content. Higher amount and/or higher LPA molar weight increase this value. These pore and mass chord-length distributions follow a negative exponential law. These exponential variations of mass and pore chords length characterize a two-phase Debye random system with sharp boundaries [21] described as 'a distribution of holes of random shape and size' [20]. We cannot conclude on the roughness of the interface (the magnification is not high enough) except for 25% LPA2 where at small distances $f_p(r)$ levels off and then falls down. A higher magnification would have lowered the number of pores taken into account leading to a non-statistic distribution. In the other cases, the curvature of the interface is lower than 20 nm.

Figs. 2(a) and (b) show the fits of $f_p(r)$ and $f_m(r)$ for 25% LPA2 with the Debye model. We observe a good agreement between experiment and theory for all LPA1 and LPA2 chord-length distributions. The observed deviation for pore chord distribution at high r-values is attributed to the big pores which are less numerous than the others leading to a non-significant statistic. Fitting the experimental results with Eq. (6) allow us to evaluate the mean lengths in porous phase $\bar{l}_p$ and mass phase $\bar{l}_m$. The lengths are not determined by averaging the chord length since we cannot take into account chords length less than two pixels (an average would have led to an overestimation of the results). Table 1

Table 1
Characteristics of the samples using chord-length distribution

	Size range of pore chords (nm)	l_p (nm)	l_m (nm)	$\bar{d}$ (nm)	Porosity Φ calculated with Eq. (3)	Macroscopic porosity P (%)
25% LPA1	31–159	14	1450	14	0.9	1.65
5% LPA2	31–116	11	1610	11	0.8	0.7
15% LPA2	27–285	22	1200	22	2.1	2.7
25% LPA2	27–655	47	1000	45	5.2	6.1
15% PVAc	21–620	36	700	34	4.9	4.2

For comparison the macroscopic porosity is indicated.

summarizes all the estimated mean lengths for LPA1 and LPA2 samples, the length $\bar{d}$, the porosity based on these values calculated with Eq. (3) and for comparison the measured porosity. As the chord-length distributions follow a Debye model (Eq. (6)), we are able to estimate lengths shorter than the minimal explored chord length value (25% LPA1 and 5% LPA2). The lengths in porous phase $\bar{l}_p$ and mass phase $\bar{l}_m$ depend on the LPA nature and content. As LPA2 content increases in the sample, the length in porous phase $\bar{l}_p$ increases and in the same time the length $\bar{l}_m$ in mass phase decreases. Adding a LPA with a lower molar weight induces a large decrease of $\bar{l}_p$. All these evolutions have to be related to the porosity amount of the sample. The porosity values based on chord-length analysis (Eq. (3)) are comparable to the measured porosity values. The porosity increases with the amount and the molar weight of the LPA. Previous works have shown similar effects [5,11]. Adding LPA favours shrinkage compensation via stresses relaxation (pores formation). The efficiency of the LPA depends on its molar weight and of the added amount and is usually estimated by the macroscopic porosity. An additional parameter, which is the length in the porous phase $\bar{l}_p$ allows describing more accurately the porosity.

A sample containing 15% PVAc was also examined for comparison purpose since this additive is widely used and studied [6,14,26]. TEM image (Fig. 4) shows a very compact network composed of microparticles (500 nm) and a sub-structure with smaller particles. A chord distribution analysis was also carried out. The pore chord-length distribution presents a negative exponential form. The pore chord length range is wide (up to 600 nm). The mass chord-length distribution presents a correlation peak for $r \approx 570$ nm (Fig. 4) attributed to crosslinked resin microparticles [11]. Such chord distribution shape in pore and mass phases are characteristic of a granular medium [19,21]. The mean length $\bar{l}_p$ in pore phase is determined by Eq. (6) since the pore chord length distribution follows a negative exponential evolution. The chord-length $\bar{l}_m$ in mass phase is determined by averaging all the recorded mass chord length since the distribution exhibits a correlation peak.

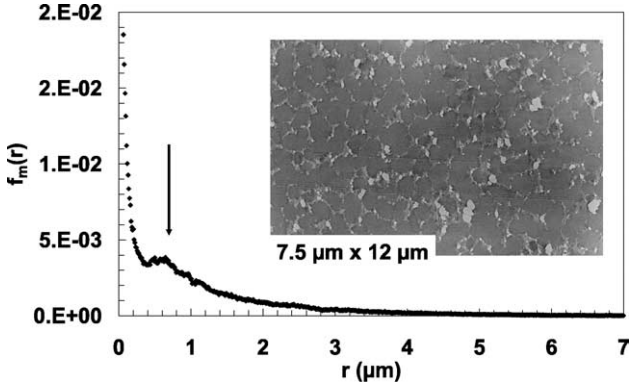

Fig. 4. Linear plot of the mass chord distribution function for 15% PVAc sample. The arrow shows the correlation peak.

3.2. Characterization of the porosity by USAXS

USAXS experiments were also carried out to characterize the porous network $I(q)$ decreases monotonously when the scattering vector increases except for UPST and 5% LPA1 sample, which exhibit two scattering peaks (these cases will be discussed later). The log–log scale plot of $I(q)$ versus q shown in Fig. 5(a) and (b) allows to observe two linear parts. Most of the scattering curves (except for 5% LPA1 and UPST samples) exhibit high-q and low-q regimes, which can be distinguished with different power-law dependencies. The low-q linear part has a slope between -1.4 and -2 and the high-q linear part has a slope between -2.5 and -4. The high-q range part corresponds to the Porod zone. The limit of this zone (q_c) gives an estimation of curvature radius of porous interface ($1/q_c$). Moreover, the large transition between the two linear parts of the curve indicates a broad dispersion of the curve radius. For each sample (Fig. 5(a) and (b)), the power-law slope in Porod zone, the limit of the Porod zone (q_c) and the associated curvature radius were measured and are summarized in Table 2. The Porod length l_C was also calculated with Eqs. (9) and (11) when the Porod's law (q^{-4} slope) is verified.

Significant progress has been made in the past years in the analysis of SAXS data based on the Porod's law [25,27]. Porod's law is indicative of an ideal two-phase system constituted by two regions (mass and pores) of constant

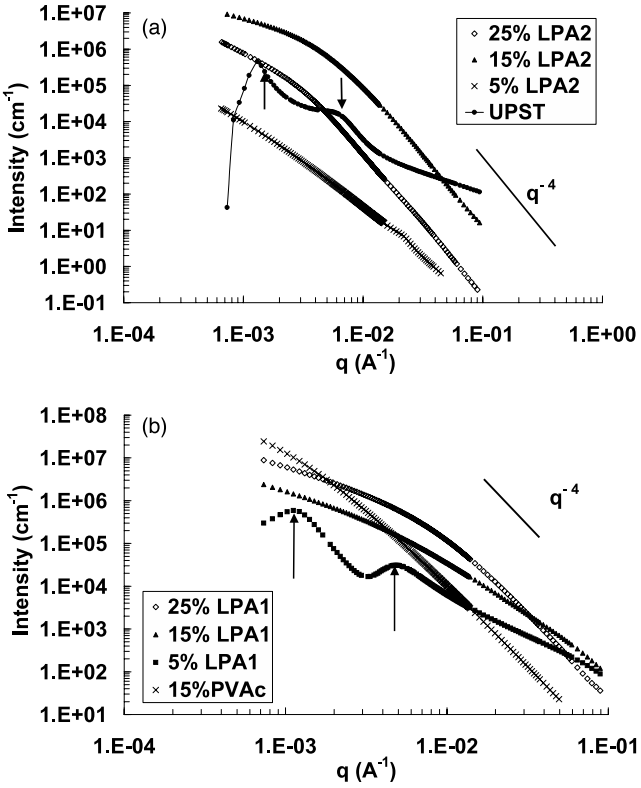

Fig. 5. USAXS scattering pattern $I(q)$ versus q in log–log scale for samples containing (a) LPA2, (b) LPA1 and PVAc. The arrows show the positions of the peaks observed for 0% LPA (named UPST) and 5% LPA1 samples.

Table 2
Characteristics determined from SAXS experiments

	Porod zone slope	Porod zone limit q_c (nm^{-1})	Porod length l_C (nm)
15% LPA1	−3.1	5×10^{-1}	–
25% LPA1	−4.0	8.2×10^{-2}	15
5% LPA2	−3.3	2×10^{-1}	–
15% LPA2	−3.9	9×10^{-2}	24
25% LPA2	−3.8	4×10^{-2}	42
15% PVAc	−3.8	3×10^{-2}	47

electronic density and an sharp flat interface. Positive deviation from the Porod's law due to density fluctuations are frequently observed. It is well-known that 1D, 2D or 3D density fluctuations in the material produce an additive positive scattering, which superimposes the q^{-4} law, thus leading to an apparent absence of the Porod's law as demonstrated for carbon materials [23]. Compositional heterogeneity within the mass has to be considered. In the present case, the mass is a blend of the cured UP/ST phase and the LPA phase. We estimated the electronic density of the cured UP/ST phase $\rho_{\text{cured UP/ST}}=1.04\times10^{11}$ cm^{-2} and the electronic density of the LPA $\rho_{\text{LPA}}=1.13\times10^{11}$ cm^{-2}.

These values are rather similar, demonstrating that the electronic contrast existing for SAXS measurements in the case of porous materials comes for a large part from a difference of electronic densities between a polymer phase (UP/St and LPA) and the porous phase. For 25% LPA1, 15% LPA2, 25% LPA2, and 15% PVAc samples, a Porod's law is observed at high-q values. The porosity of these blends is large higher than $\Phi=2\%$ and the scattered intensity comes essentially from the electronic contrast between the solid phase and the porous phase. The solid phase is seen as a region of constant electronic density. The limit of the Porod zone, first approximation of curvature of the interface increases with weight percentage and/or with molar weight of the thermoplastic additive. The Porod length, when the Porod's law is observed, does not exceed 47 nm. l_C is also highly dependent of the LPA content and LPA molar weight: it strongly decreases with a lower molar weight (at a given wt%) and lower weight percentage.

Other samples (15% LPA1, 5% LPA2) with a low porosity ($\Phi=0.7\%$) exhibit a slope between −3 and −4 in the largest q regime. For 15% LPA1 and 5% LPA2 the slope is respectively −3.1 and −3.3. Such results could be interpreted as a consequence of a rough interface at this scale or could be considered as a deviation of the Porod's law due to superposition of ideal Porod's law and density fluctuations. However, in the case of 5% LPA2 sample, the pore chord distribution function shown in Fig. 3(b) is essentially exponential in the length domain where Porod deviations are observed (on the order of π/q). An algebraic dependence with r is expected in the case of a rough self-affine surface [19]. So, it appears doubtful that the positive deviation from the Porod law is due to surface roughness. Consequently, the positive deviation observed in our case has to be related to density fluctuations in the polymer phase. For the considered samples, it is clear that the porosity is low and consequently the intensity of the scattering due to density fluctuations can interfere strongly the scattering intensity due to mass/pores interface.

In two peculiar cases (5% LPA1 and UPST), two relative maxima are observed over the whole scattering range. In the case of 5% LPA2 a weak maximum could also be observed. Such results indicate that correlation lengths exist in the sample. The corresponding scattering vectors are $q_1=1.3\times10^{-2}$ and $q_2=6.9\times10^{-2}$ nm^{-1} for UPST, $q_1=1.1\times10^{-2}$ and $q_2=5.1\times10^{-2}$ nm^{-1} for 5% LPA1. The values of q_1 and q_2 are quite similar from one sample to another. No harmonic relation exists between q_1 and q_2 suggesting that there is no relationship between these peaks. The macroscopic porosity of UPST and 5% LPA1 samples are 0 and 0.5%, respectively, implying a non-significant contribution of the porosity to the scattering pattern. The scattering intensity is only due to compositional heterogeneities. We suggest that q_1 peak comes from crosslinking heterogeneities as depicted in the literature [3]. q_2 peak could be a mark of phase separation frozen by gelation since the corresponding correlation length is close to the period of the concentration fluctuations observed during in situ experiments [11].

4. Discussion

SAXS results and chord distributions give two different insights into the porous developed medium. Chord length distributions show that for LPA1 and LPA2 the porous medium is within a given scale a random Debye medium. The length $\bar{d}$ is thus obtained from chord-length distributions. SAXS experiments allow investigating the nature of the porous interface. When the porous interface is flat at high-q range and the Porod's law can be applied, an estimation of the Porod length is thus obtained. The length $\bar{d}$ and the Porod length l_c have to be compared. For most of the porous samples, the lengths obtained by SAXS are similar with those obtained from chord distributions (Tables 1 and 2). The pores in these cases are large enough to appear with a flat interface at high q-range for SAXS investigations. For 5% LPA2 and 15% LPA1, SAXS deviation from the Porod'law does not allow the determination of the Porod length. In these two cases the Porod zone limit, which defines a limit of the investigation of the interface for high q-range is less than 5 nm.

It is highly interesting to relate these pore characteristics to the nature and mechanism of the phase separation between the LPA-rich phase and the UP-rich phase (crosslinked UP/St molecules). This phase separation indeed governs the pores apparition [2,13,14,28]. As the crosslinking of UP/ST induces a significant shrinkage (8–10%), stresses are generated within the sample. These stresses can be released by pores formation only when

interfaces are developed in the sample (point of low mechanical resistance) via phase separation. Neat UP/ST system undergoes macroscopic shrinkage without pore formation. During curing, the blend with LPA undergoes successive stages. The first one is the phase separation, which arises for a conversion degree lower than 0.1. As we have shown in a previous study [11], the phase separation proceeds via spinodal decomposition, which creates interfaces between LPA-rich phase and UP-rich phase. In situ SANS and USAXS demonstrated that gelation freezes the phase separation, leading to a co-continuous biphasic system (LPA-rich phase and UP-rich phase). The nature of the interface (diffuse or sharp interface) between the two phases is governed by LPA content and its chemical nature. More precisely, the key factor is the relative position of the gelation and the phase separation onset, which is governed by the miscibility parameter of the initial blend. A low LPA content and/or a low molar weight lead to a system where concentrations fluctuations still subsist at the end 'with a diffuse interface'. This was related to the close position of the phase separation onset in respect to the gelation. Higher LPA content and/or a higher molar weight allow an earlier onset of the phase separation, implying the formation of sharp interface. This is illustrated in Fig. 6. For a conversion degree higher than 0.5 [4], pores appear at points of lower mechanical resistance—namely at the interface between LPA-rich phase and UP-rich phase. Consequently, a sharp interface between these two phases will favour porosity formation and pores with flat interface. A diffuse interface will prevent from pore formation: only small pores are observed; eventually no porosity can be observed at all.

5. Conclusion

These results give new insight into the description of the morphology of thermoset blends based on unsaturated polyester. In addition to the bulk morphology which is widely used to depict the cured materials (i.e. size of the particles and aggregates) pores characteristics were considered in this study. Thanks to the determination of mean lengths within the materials, pore sizes were estimated allowing a more extensive description of the porosity. Usually, only the macroscopic pore content is considered.

The chord length distribution helps in this characterization by giving the possibility of describing the morphology of porous medium. In our case the random character of the porous medium (Debye model) within a given scale is demonstrated. A length $\bar{d}$ is also determined for the different samples and is lower than 47 nm. SAXS experiments give an approach of the nature of the porous interface. These two approaches of the porosity are complementary by giving different insight on the characteristics of the pores and also concordant since the characteristic lengths determined by SAXS and chord distribution analysis are quite similar.

Thanks to these approaches we herein confirm the strong influence of the LPA type and amount on the porosity. We indeed demonstrated that in addition to macroscopic amount of porosity variation, characteristics of the pores are largely influenced. Large pores, with flat interface patterns (SAXS patterns at large angles follow Porod's law) are formed for high content and/or high molar weight of LPA. For low content and/or low molar weight of LPA, the deviation from q^{-4} dependence on SAXS measurements could be attributed to an additional positive scattering induced by density

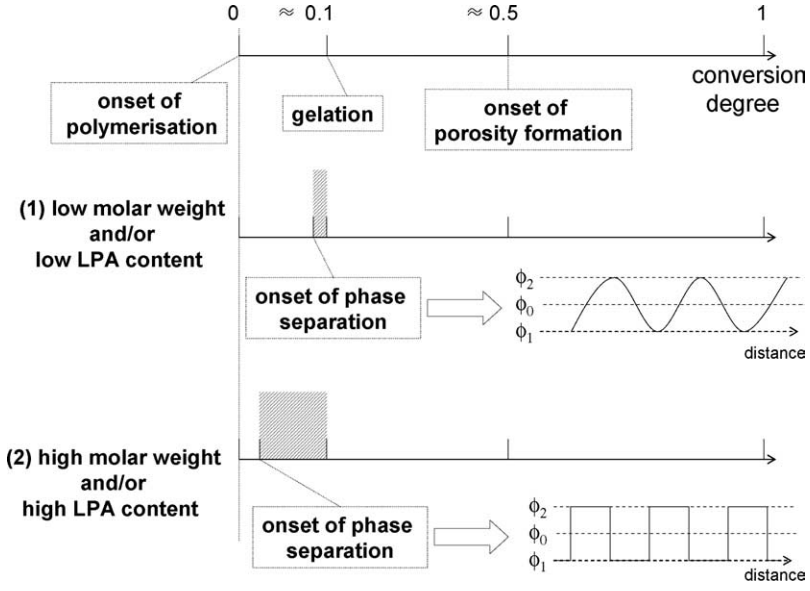

Fig. 6. Schematic diagram of the successive phenomena occurring during polymerisation. The concentration fluctuations are correlated with the position of the onset of the phase separation in respect to the gelation which stops further evolution. Diffuse interface is obtained in the first case (1) whereas sharp interface is found in the second one (2).

fluctuations. This has to be related to previous results showing the dependency of the morphologies of the separated domains generated during the reaction with the initial miscibility properties of the blends.

Acknowledgements

This work was financially supported by 'la region Centre' and the Menzolit Company. The authors would like to thank O. Spalla from CEA DRECAM/SCM (Saclay, France) for USAXS experiments, J. Teixeira from CEA LLB (Saclay, France) for fruitful discussions and D. Jalabert for TEM experiments.

References

[1] Bartkus EJ, Kroekel CH. Appl Polym Symp 1970;15:113.
[2] Li W, Lee LJ. Polymer 2000;41:697.
[3] Pascault JP, Sautereau H, Verdu J, Williams RJJ. Thermosetting polymer. New York: Marcel Dekker Inc; 2002.
[4] Boyard N, Vayer M, Sinturel Ch, Erre R, Delaunay D. J Appl Polym Sci 2004;92:2976.
[5] Vayer M, Serré C, Boyard N, Sinturel C, Erre R. J Mater Sci 2002;37: 2043.
[6] Huang Y-J, Liang C-M. Polymer 1996;37(3):401.
[7] Serré C, Vayer M, Erre R, Boyard N, Ollive C. J Mat Sci 2001;36:113.
[8] Kinkelaar M, Wang B, Lee LJ. Polymer 1994;35:3011.
[9] Zhang Z, Zhu S. Polymer 2000;41:3861.
[10] Inoue T. Prog Polym Sci 1995;20:119.
[11] Boyard N, Sinturel Ch, Vayer M, Erre R. J Appl Polym Sci 2004 [in press].
[12] Zheng Q, Tan K, Peng M, Pan Y. J Appl Polym Sci 2002;85:950.
[13] Suspène L, Gerard J-F, Pascault J-P. Polym Eng Sci 1990;30(24): 1585.
[14] Suspène L, Fourquier D, Yang Y-S. Polymer 1991;32:1593.
[15] Chan-park MB, McGarry FJJ. J Adv Mater 1995;27:47.
[16] Brown GM, Butler JH. Polymer 1997;38:3937.
[17] Lambard J, Lesieur P, Zemb T. J Phys I, France 1992;2:1191.
[18] Mering J, Tchoubar D. J Appl Cryst 1968;1:153.
[19] Levitz P, Tchoubar D. J Phys I 1992;2:771.
[20] Debye P, Anderson Jr HR, Brumberger H. J Appl Phys 1957;28:679.
[21] Levitz P. Adv Colloid Interface Sci 1998;76–77:71.
[22] Debye P, Bueche AM. J Appl Phys 1949;20:518.
[23] Ruland W. J Appl Crystallogr 1971;4:70.
[24] Sinha SK, Sirota EB, Garoff S, Stanley HB. Phys Rev B 1988;38: 2297.
[25] Smarsly B, Antonietti M, Wollf T. J Chem Phys 2002;116:2618.
[26] Hsieh YN, Yu TL. J Appl Polym Sci 1999;73:2413.
[27] Burger C, Ruland W. Crystallogr Acta Sect A 2001;57(Part 5):482.
[28] Atkins KE, Koleske JV, Smith PL, Walter ER, Matthews VE. 31st Annual technical conference, 1976.